Submitted: 01/13/2024
Accepted: 03/08/2024
Published: 04/05/2024

Research Article

[1]Department of Bioengineering, McGill University, Montréal, QC, Canada

[2]Department of Mechanical Engineering, McGill University, Montréal, QC, Canada

[3]Department of Electrical Engineering, McGill University, Montréal, QC, Canada

[4]Department of Computer Engineering, McGill University, Montréal, QC, Canada

Keywords

Orthopedic implants, finite element analysis, vibrations, space travel

Email Correspondence

rocketteam.payload@mcgilleus.ca

https://10.26443/msurj.v19i1.221



Chloe Jacquet[1], Jay Patel [2], Pierre Khoury [3], Xingbo Huang [2], Theodore Glavas [4]

# Orthopedics in Space Travel: Developing Procedures to Evaluate the Safety of Implants Amidst the Rise of Commercial Space Tourism

## Abstract

With the rise of commercial space tourism, the barrier to entry into space lowers. Therefore, passengers with more complex medical conditions are predicted to enter space. This report aims to initiate the development of procedures assessing the safety of space travel for individuals with orthopedic implants. In preparation for the 2023 sounding rocket launch by McGill Rocket Team, the Payload subteam developed a bone model, a human model, a finite element analysis model, and a testing model to determine the safety of orthopedic implants under the harsh conditions of spaceflight. Measuring the dynamic forces of the MRT's *Porthos* rocket in flight yielded vibrations in the 300–2750 Hz range, which is valuable for creating better models of the loading conditions on orthopedic implants in silico. Three point bending testing revealed high precision but low accuracy in measuring the mechanical strength of the models. Ultimately, the study recommends adjusting the testing models to prevent oversimplification. Future work should analyze bone screw interfaces on a microscopic level to detect small changes in implant stresses. By implementing these changes, procedures can accurately describe the safety of spaceflight for those with orthopedic implants.

## Introduction

### Orthopedics in space travel

In the age of Blue Origin, Virgin Galactic, Rocketplane Global, and other novel commercial spacecraft companies, space tourism is revolutionizing space travel[1]. As the industry grows, we expect a rise in passengers entering space with increasingly diverse medical backgrounds. This will require protocols that evaluate the safety of spaceflight for passengers with different medical conditions. Although we project an increase in this type of research in the coming years, the literature is currently limited. Within the context of orthopedics, it is largely under-researched.

This paper introduces methods to study the impact of flight conditions on the strength of an orthopedic device. The results lay the groundwork for developing future procedures that assess whether individuals with orthopedic implants can safely travel to space. These procedures will hold important implications in both the commercial and professional space industries. Commercially, since orthopedics are often permanent implants, our research questions the accessibility of space travel within a rapidly expanding industry. Professionally, it can help agencies evaluate the risks of potential emergency procedures involving orthopedic implants for use in long-term missions.

### McGill Rocket Team

The McGill Rocket Team (MRT) is an interdisciplinary student-led design team tasked with designing and launching a sounding rocket each year. Sounding rockets are designed to complete scientific research in a sub-orbital trajectory[2]. This research is encapsulated in the rocket's payload. Each year, MRT's Payload team designs a scientific experiment that leverages the unique conditions of spaceflight. During the 2023 launch in Timmins, Ontario, the team launched the payload LOVE (Launching Orthopedics Vibration Experiment) on MRT's *Porthos* rocket at an apogee of 2400 m. LOVE was MRT's first attempt to initiate research in the sphere of orthopedics within space travel. This paper presents the experiment's findings and discusses methods for assessing the safety of orthopedic implants in space travel, as well as how to evaluate the quality of these methods.

## Model Development

### Bone Model

For pilot testing, long bone screw-plate fixations were chosen due to their simple modeling and high failure rates[3]. High clinical failure rates were optimal for modeling as the team aimed to evaluate the most vulnerable orthopedic fixations. The independent variable in the study was bone density. Decreased bone density, otherwise known as osteopenia, is a widely

observed phenomena amongst astronauts subjected to long periods of decreased gravitational forces, particularly in load-bearing bones like the tibia[4]. With this in mind, models of both healthy and osteopenic bone were included in the payload. Bone consists of two distinct components: the outer cortical layers and the inner cancellous tissues. Cortical bone is hard and stiff with high mechanical properties, whereas cancellous bone is soft and spongy with low mechanical properties. Therefore, the biomechanical contributions of cancellous bone were considered negligible and excluded from the model. Nevertheless, bone loss manifests differently in the two bone components. Whereas cancellous bone uniformly increases porosity in response to osteoclast dominance, cortical bone resorption occurs primarily on the innermost layer[5,6]. As a result, osteopenia presents as cortical thinning, which we simulated by decreasing the cortical thickness of the bone samples.

Another component of the bone model is the fracture type. Depending on the mechanism of injury, three common fracture types can occur: simple, wedge, and complex[7]. For feasibility, only simple fractures were considered. Complex fractures, such as spiral fractures, often require more intricate internal fixations, which is beyond the scope of our abilities[7]. Wedge fracture patterns vastly complicate modeling and would prevent thorough and substantial pre-flight modeling. Therefore, a simple fracture was modeled in the diaphyseal portion of the tibia. To simulate the least stable fixation condition, oblique fractures were modeled where transverse fractures have higher mechanical stability. Since oblique fractures most commonly range between 10–40 degrees from the horizontal axis[8], we selected a 23 degree angle to maximize instability without interfering with the screws.

When selecting a bone material, the team considered three options as human bone analogues: animal bones, 3D printed segments, and composite biomechanical models. To simulate the mechanical strength of bone most accurately, the team prioritised a close match on Young's modulus and cortical thickness. Human cortical bone has a Young's modulus of around 16 GPa[9]. Common animal bones have both a larger cortical thickness and a lower Young's modulus compared to humans[10]. Furthermore, the Payload could only fit four samples: two healthy and two osteopenic models. Due to the experiment's limited repetition, inconsistencies between samples would thus introduce too great an uncertainty, disqualifying the animal bone. Traditional 3D printing methods were also unsuitable as they could not achieve the necessary Young's modulus[11]. Consequently, the team selected Sawbones glass fiber epoxy composites from Pacific Research Laboratories, for their accurate simulation of the biomechanical properties of cortical bone with a Young's Modulus of 16 GPa[12]. For order of magnitude validation, the same experiment was performed on juvenile bovine tibias. These were tested against the control and flight samples.

## Human Model

The payload's structure was designed to incorporate the orthopedics experiment, particularly how the bone analogs would connect to the structure. During this design phase, the team had to make assumptions to simplify the anatomical bone model, making the project feasible within time and space constraints. The first assumption regarded the biomechanics of the joints surrounding the tibia, which largely determine the forces felt by the bone and ultimately describe the effects of flight on the bone. However, due to the small space in the payload (roughly 10 by 10 by 25 cm), the joints had to be simplified to fit multiple samples. Through consultation with the McGill Orthopaedics Research Laboratory (ORL) and McGill Musculoskeletal Biomechanics Research Laboratory, the team found that the knee-tibia joint acted like a pinned or hinged connection, while the tibia-ankle joint acted as a fixed connection. Similarly for space constraints, the team chose to ignore the mass and mechanical properties of the flesh surrounding the tibia. This flesh is made up largely of the gastrocnemius muscle and the attached Achilles tendon, which lie at the back of the leg. Through comparison of their Young's moduli (440 kPa compared to 16 GPa), the flesh is more than $10^4$ times weaker than the tibia's cortical bone, or the bone analogs used in this experiment[9]. This justifies the choice to ignore the muscles and tendons surrounding the tibia in our payload, as they do not have a significant effect on the strength of the sample. These two assumptions, to simplify the joints and ignore the flesh, allowed for a total of four fractured and plated samples in the final payload.

One of the experiment's design variables was the angle at which to hold the bones at during flight. Since the force would be transferred into the samples through vertical acceleration (G-forces) and vibrations from the engine, this orientation variable was extremely important to define. The team researched how astronauts sit in human-rated capsules, like Blue Origin's suborbital New Shepard[13]. The team determined that an angle of 25 degrees from the horizontal would replicate seating conditions closely. These assumptions and simplifications led us to the final design of our structure (Figure 1).

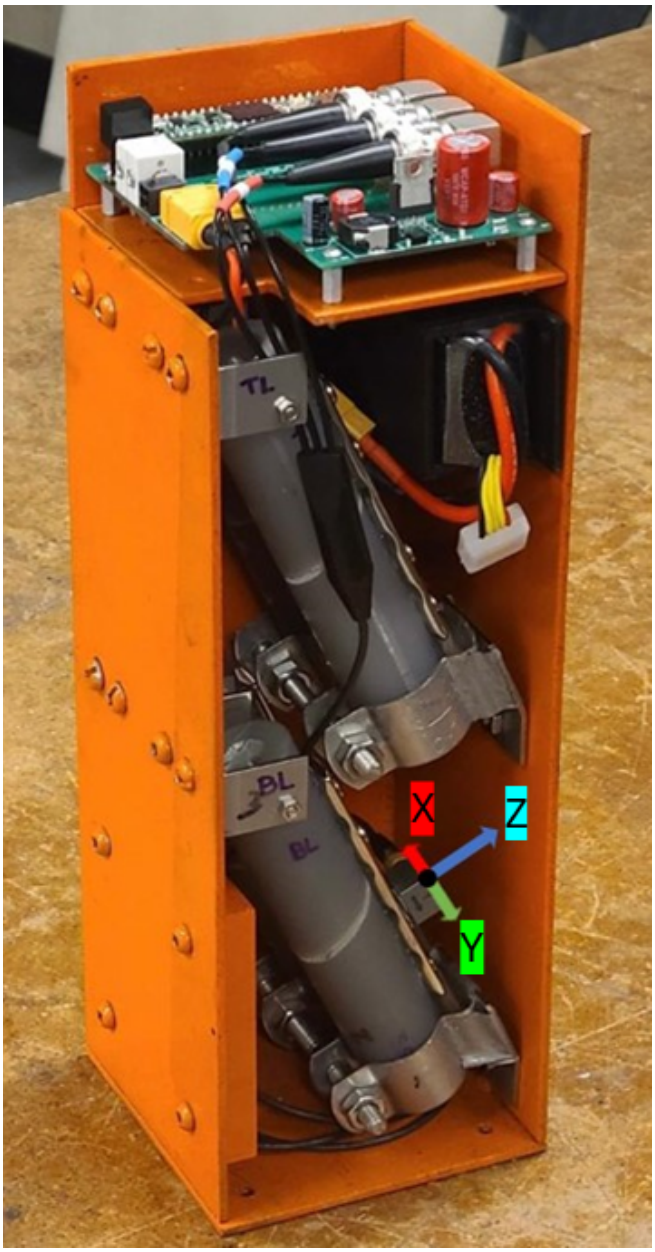


**Figure 1.** Finalized structure of the Payload with labelled *x*, *y* and *z*-axis of the Accelerometer where *x*-axis points into the bone, *y*-axis points along the DCP orthopedic plate and Z points in the direction perpendicular to the DCP orthopedic plate.

### Force Model

A rocket environment demonstrates two distinct types of acceleration: dynamic and linear. Dynamic acceleration results from the vibrations and shaking of the rocket, whereas linear acceleration is generated by the upward thrust of the rocket. To have a comprehensive understanding of all the forces acting on the bone model, both dynamic and linear acceleration must be studied.

The top compartment of the Payload contained a student-developed Vibration Data Acquisition (DAQ) System (Figure 1). This custom Printed-Circuit Board (PCB) was used during the August 28, 2023 flight to acquire vibrations data by powering the 3 axial vibrational accelerometer and conditioning its output signal. The accelerometer was an Integrated Electronics Piezo-Electric (IEPE) sensor specifically suited for the aerospace industry, generously provided as a sponsorship by Hottinger Brüel Kjaer Inc. It specializes in accurately measuring dynamic acceleration and omits linear accelerations. As the PCB also contained a linear accelerometer, all acceleration types were measured.

Studying the vibration effects of the rocket environment on an orthopedic implant cannot be accurately replicated in a laboraty setting. Although there exist vibration testing equipment such as a shaker table, it has a set of limitations. NASA's space-grade shaker tests consist of a sinusoidal sweep test and a random vibration test. These tests create uniformly distributed vibrations to the device under test. However, in-flight conditions are harsher than simulated environments, and rockets are subject to forces of differing magnitudes[14]. Furthermore, shakers can only generate acceleration along a single axis at a time, whereas during flight, acceleration occurs in all degrees of freedom simultaneously. Perhaps the greatest limitation of a shaker test is its inability to properly simulate a shock event, a big burst in energy in a short amount of time. Shock events such as rocket engine fire or a stage separation are extremely common in rocket launches and correspond to events when mechanical stresses are extremely high.

### Finite Element Model

Before performing the experiment by launching the rocket, the team used finite element analysis (FEA) to predict the effects of the different conditions in the rocket to help experimental design. When used correctly, FEA can identify areas of larger stress, deformation, and modes of vibration, providing prelimary knowledge to aid in experiment setup. A pre-launch analysis was also performed using FEA to confirm that the bone and plate assembly would not fail catastrophically under the loads experienced in the rocket. A set of hand calculations confirmed this. Using Siemens NX Nastran software, the team made several assumptions related to the material and the bone-plate assembly. In the initial computer model, the bolts connecting the bone and plate together were removed entirely and replaced with a gluing condition holding the plate to the bone, along with pinned conditions in the bolt holes. This simplification was feasible as the strength of the metal bolts far exceeded that of the bone, allowing them to be replaced with infinitely strong pins. This simplified the analysis, allowing us to create higher resolution and therefore more accurate results for stress concentrations in the bone. The fixed-pinned end conditions were modeled with a fixed constraint at one end and a pinned constraint at the other, which assumes the connections to the bone are rigid and frictionless. Once again, the designed metal fixtures to hold the bones at each end were far stronger than the bones themselves, so we did not expect significant deformation or damage in the end fixtures. The Sawbones models had a listed density of 1.64 g/cm$^3$, Young's modulus of 16 GPa, and a Poisson's ratio of 0.26 [12]. These were used to create a custom material in NX Nastran FEA, which remained the bone material throughout the analyses (Figure 2a).

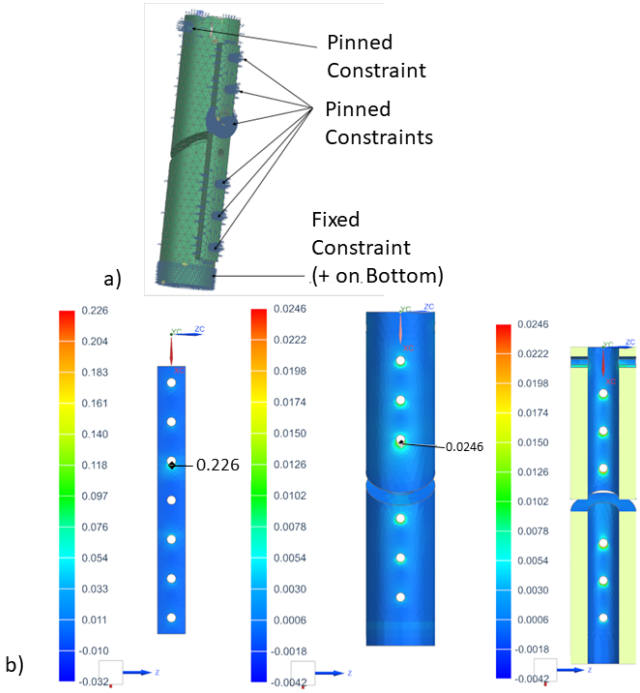


**Figure 2.** a) The meshed FEA model with all assumed constraints b) Results of the static FEA under launch conditions

## Methods

### Vibration Instrumentation

The Data Acquisition (DAQ) PCB measures the dynamic acceleration of the system. To optimize measurement accuracy, the DAQ PCB was calibrated according to the expected frequency and acceleration amplitude range. These parameters were obtained by testing the rocket engine, which is the main source of vibration. Through a series of engine tests, the team confidently assumed that all vibrations would range between 100 to 5000 Hz. These measurements correlated with what is observed by typical sounding rockets. The frequency range of the DAQ system was then limited, thus optimizing sampling precision and accuracy comparably with controlled vibration sources.

### Finite Element Model Validation

The pre-launch analysis using FEA provided the team with insights into in-flight conditions. FEA involves making a computer model, with assumptions and simplifications as described in the previous section, that is then broken up into small mesh elements (meshed). In static analysis, the acceleration conditions of the rocket at both launch and parachute deployment are given to the program and applied to the elements. The program then outputs a coloured model displaying the stresses felt throughout the model. Viscoelasticity was not considered for our FEA model as the glass transition temperature was not made apparent by the supplier. Through iterative refinement of the mesh, we developed a static FEA model that applied a downward acceleration of 10 Gs and held the bones at 25°, which matched the experiment set-up. The results are shown in Figure 2b). The maximum in-plane stresses were 226 kPa and 24.6 kPa for the plate and bones, respectively. Both stresses were located around the hole directly above the fracture. These results are far below the yield stresses for the plate (275 MPa) and cortical bone (51.0 MPa). The same analysis was then repeated with the acceleration direction instead pointing up to simulate parachute deployment. With this change, similar stress values were calculated but the area of high stress was re-situated to the hole directly below the fracture.

Since the rocket's ascent subjects the bones to vibrations from the engine, we decided to conduct a normal modes vibration analysis. This analysis aimed to identify the natural frequencies of vibration and their corresponding mode shapes. The first ten modes of vibrations were between 1.182 kHz and 4.425 kHz, with shapes varying between longitudinal and torsional vibrations.

A limitation of this study is that it precludes damping. In reality, mode shapes are expected to be lower due to stress and deformation. However, this analysis does help identify areas of high stress, such as at the pin connection at the top of the bone (the knee-tibia interface), and the first four bolt holes closest to the fracture. These simulation results agree with solid mechanics theory, which states that stress tends to concentrate around holes or interruptions in 'stress flow[15].'

### Determination of Natural Frequency of Continuous Systems

The upper bound of the natural frequency of a continuous mass system can be approximated using Rayleigh's method as described below:

$$\omega_n^2 \leq \frac{\int_0^L EI\left(\frac{d^2y}{dx^2}\right)^2 dx + \sum_{i=1}^n m_i y_i}{\int_0^L my^2\, dx + \sum_{i=1}^n m_i y_i^2}, \quad (1)$$

whereby $\omega_n$ is the natural angular velocity, $m_i$ and $m$ are the lump mass and continuous mass per unit length, $E$ is the elastic modulus, $I$ is the second moment of area, $L$ is the length of the orthopedic plate, $y_i$ is the static displacements induced by the lump masses, and $y = y(x)$ is the global shape function given by

$$y(x) = y_0(L^3 - 3Lx^2 + 2x^3) \quad (2)$$

for pin-fixed boundary conditions, whereby $y_0$ is a constant.

### Preparing models and animal samples

Eight models were constructed, four healthy and four with osteopenia. Each model was 12.0 cm in length with an outer diameter of 27.0 mm. The healthy samples had an inner diameter of 13.0 mm and the samples with osteopenia had an inner diameter of 17.0 mm. This is because a 2.0 mm change in cortical thickness per side follows the estimated maximum decrease in cortical thickness observed for an ageing subject with no other health problems[16]. Two healthy samples and two samples with osteopenia were flown in the rocket and the remainder were used for control testing.

The fixation of the fractured bone segments was completed under the supervision of an orthopedic surgeon. A 1.3 mm fracture gap was maintained to further destabilize the interface. The two fragments were arranged such that they were separated by a 1.3 mm washer in a bench vise. Beginning with the center most hole, a 3.5 mm cobalt drill with a surgical drill guide was used to bore completely through both cortices. The 4.5 mm self-tapping screw was tightened using a hex screwdriver. This was repeated for the remaining holes. There was slight translation and torsion of the bone fragments during the first plating. To prevent downward translation of the second fragment, an upward force was applied to the bottom of the fragment while drilling. To prevent torsion of the plate, the vise was further tightened and the plate was clamped on both ends.

### Post-Launch analysis

To assess the impact of the rocket launch on the bone segments post-launch, we subjected the flown samples and control samples to mechanical testing. During healing, bones are subjected to three major loading conditions: axial loading, bending, and torsion. Due to the seating orientation during ascent and descent, the tibia was assumed to be primarily subjected to bending. Both samples were fixed at the ends, thereby minimizing motion in the *x* and *y*-axis. However, the pinned configuration imposed no moment along the bone axis that would have allowed for bending. As the leg is typically securely fastened during ascent and landing, torsion forces were assumed to be minimal.

The greatest changes in mechanical strength were therefore predicted to be in the bending modulus. The model's variation in strength was characterized by performing 3-point bend testing on the plate/fracture interface. The control models were tested before flight and the experimental models were tested after recovery.

In accordance with industrial conventions, the international standard of regulatory testing (ISO 178) was adapted for the purposes of biomechanical testing[17]. The flexural properties of rigid and semi-rigid materials during 3-point bending are detailed in ISO 178. The bending modulus was extracted from the stress strain curves and used to characterize the effects of the measured vibrations and forces.

## Results

### Launch Outcome

The results presented below were gathered using the Vibration Data Acquisition System described in the methods section above. The data presented is based on the 3-axis shown in Figure 1. Due to human mishandling, the *z*-axis connector was not properly connected. As a result, no vibration data was collected on that axis.

The 150-second flight contained three unique flight events: engine burn, drogue deployment, and landing. The results presented in the subsequent paragraph will focus on these engine burn event as a means of demonstrating the type of data collected.

Vibrational data can be presented in the time domain, the frequency domain, and spectrographically. The time domain representation is used for looking at a vibration, such as a shock event, over a small interval of time. Data can be observed in the frequency domain by plotting a Fast Fourier Transform (FFT), acquiring a broad overview of the vibration amplitude as a function of frequency. Viewing the data in the frequency domain allows us to understand the vibration profile of the rocket by highlighting the main frequency modes. Finally, the spectrogram is a series of FFTs over time. This data representation shows the evolution of the frequency response of the rocket over time. This is especially useful in a changing environment such as a rocket, where different mechanical phases are present. In the case of rockets, the frequency domain and spectrographic representations offer the best visuals of the vibrations.

The engine burn lasted roughly 20 seconds. The vibrations observed are up to 35 m/s$^2$ in the *x*-axis and up to 80 m/s$^2$ in the *y*-axis, with an overall range of 300–2750 Hz. It had a dominant mode of 1500 Hz and secondary modes (harmonics) at 500 Hz and 2500 Hz, thus confirming the frequency range assumptions made while calibrating the DAQ system. This data for the *x*-axis is conveyed in the frequency domain and spectrogram graphs which can be found in Figure 3 and 4, respectively.

### Natural Frequency Calculation

Data was acquired through an accelerometer located at the midspan of the orthopedic plate on one of the four samples. The sample is assumed to be symmetric along the circumferential direction. Specifically, two time-series acceleration datasets were taken at the accelerometer location in the *x* and *y* directions, as depicted.

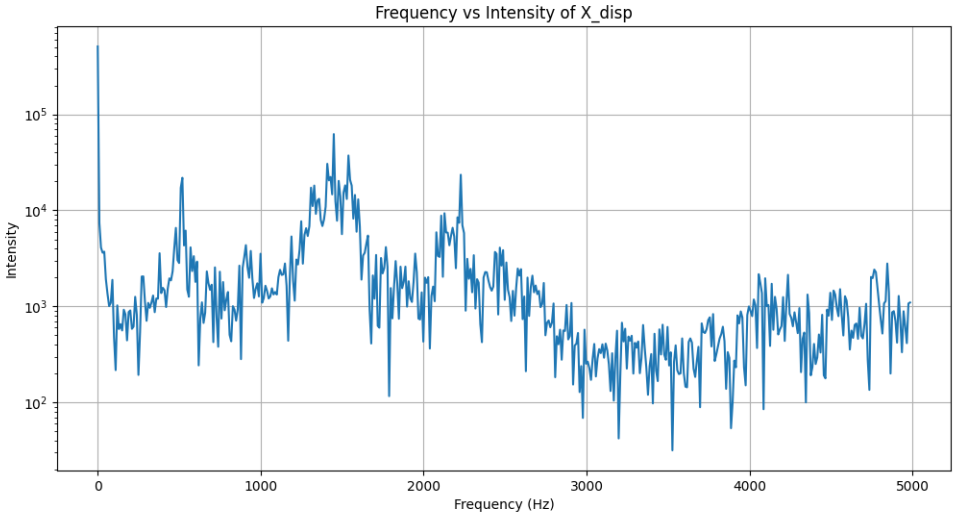


**Figure 3.** Frequency vs. Intensity graph of accelerometer data.

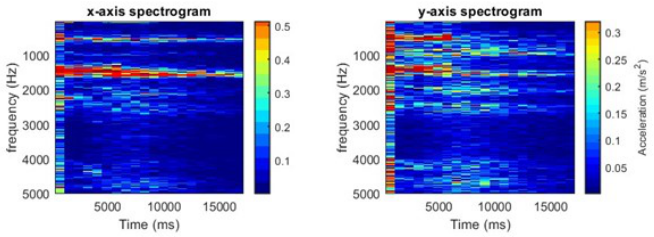


**Figure 4.** Spectrogram for engine burn for the *x*-axis (left) and *y*-axis (right).

Using the specifications of the healthy bone sample and the orthopedic plate, we obtain from Equations 1 and 2 an estimated upper limit for the first natural vibration angular velocity of $\omega_n \leq 2405.1$ rad/s or a natural frequency of $f_n \leq 382$ Hz.

### Bend Testing

No significant difference was observed between the mean flexural strength of the flown and control samples. Further, no significant differences were observed between the mean flexural strength of the healthy samples versus those with osteopenia. However, the values measured for the juvenile bovine tibias had very high variability and were significantly lower than the composite samples (Table 1).

**Table 1.** Calculated Bending Modulus of the juvenile bovine samples, and the pre- and post- flight Sawbones samples.

| Sample Type | Sample 1 (MPa) | Sample 2 (MPa) | Sample 3 (MPa) | Averaged Value (MPa) |
|---|---|---|---|---|
| Juvenile Bovine | 123 | 219 | 167 | 169.7 |
| Healthy Pre-Flight | 298 | 276 | - | 287.0 |
| Osteopenic Pre-Flight | 244 | 277 | - | 260.5 |
| Healthy Post-Flight | 268 | 276 | - | 272.0 |
| Osteopneic Post-Flight | 283 | 294 | - | 288.5 |

## Discussion

### Model Evaluation

As observed in the bending results, the composite Sawbones models allowed for very precise results. The variability between trials was maximized at 30 MPa for the osteopenia-affected control samples, and minimized at 11 MPa for the osteopenia-affected test samples. This is much lower than was observed in the juvenile bovine samples, with a 96 MPa difference in the bending modulus between samples 1 and 2. The composite models were therefore ideal for the constraint of limited repeatability. The procedures for preparing the models are concluded to have been ideal for maximizing precision and use of space. However, the accuracy of the model was sacrificed by an oversimplification based on our limitations.

The lack of variance between the healthy samples and those with osteopenia indicates an issue with the model's evaluation of mechanical strength. Literature supports that bone density has significant impact on tibial mechanical strength[18]. Therefore, we conclude our method of three point bending was not an effective procedure for measuring mechanical strength. During testing, the stainless steel orthopedic plate yielded before the bone, meaning any deterioration that occurred in the bone itself was not measured.

Subsequently, the results between the flown and control models are invalidated. This could also be attributed to the bone model used. We hypothesize that neglecting the cancellous bone and focusing on the diaphyseal tibia was an oversimplification. The diaphyseal tibia is the strongest section of the bone with the most cortical tissue[16]. This section is therefore the most stable location for a screw fixation. Further work should analyse cancellous bones in sections with lower cortical composition like the epiphysis, where weakening is most likely. The results also implicate that macroscale analysis is not sufficient to understand the strength of the interface. This is supported by the FEA results which predicted minimal changes after flight. Small changes in compressive forces can have significant implications including induced apoptosis, increased resorption, reduced vascularization, and microfractures[19]. By analyzing cancellous bone on the microscale, small changes in compressive forces can be measured. The implications of these forces can be estimated in reference to existing literature.

The material we chose could also have affected the accuracy of the results.

The Sawbones composites accurately modelled the bulk of the mechanical properties of the cortical bone, but they were unable to represent microstructures and porosity. For analysis on the microscale, real bone internal geometries should be used to accurately represent the interaction with the screws. In the Sawbone model, the screw is completely engaged with the composite at all positions. In cortical bone, the porosity of the material would change the thread engagement. Using real bone samples can accurately represent this interaction.

The human model must also be re-evaluated. The assumption of a cylindrical structure negates the effects of stress concentrations. In reality, the tibia is not a perfect circle and the cortical thickness is not uniform. Stresses would not be uniformly distributed within the bone, allowing for failure modes in areas of high stress concentration.

We can also compare the FEA predictions from pre-flight to the observed forces during flight. From Figure 3, it can be seen that the FEA excitation frequency range of $1182 - -4425$ Hz does not fully bind the accelerometer excitation frequency, meaning there was some error in approximating the first vibration mode. However, the dominant vibration frequency observed at 1500Hz was correctly identified. The FEA performed for vibration analysis can be further improved through the use of more accurate forcing conditions for the acceleration phase, as well as the use of other deformable solid models that more closely resemble our orthopedic sample.

The observed frequency dominant vibration frequency is significantly higher than the theoretical natural frequency from Equation 1, of the first mode of 382 Hz. This suggests that the operating frequency range with external forcing from acceleration does not instill any resonance phenomena. Forced vibration analysis FEAs can be performed in future works in reference to the accelerometer data and the discovered excitation frequencies.

### Limitations and future work

As a pilot study, LOVE provided insight into quantifying the effects of spaceflight forces and vibrations on the stability of orthopedic implants. Using the lessons learned from this study, the payload team will implement a microscale analysis on screw insertions in cancellous bone in next year's payload. Further, the vibration profile collected from the first flight will allow predictive analysis using FEA to estimate the effects of the launch on next year's model.

## Acknowledgments

Writing this paper would not have been possible without all the talented students in the McGill Rocket Team who succeeded in launching and recovering a rocket, a first for all who were involved. A special thank you to the Payload subteam for bringing LOVE to life, as well as to all our advisors and sponsors who supported us throughout the journey: Thank you to Dr. Peter Glavas for sharing your expertise in orthopedics, as well as to Dr. Ahmed Aoude and Dr. Emily Newell for your valuable feedback. We are grateful to Nikita Letov & Lucie Riffard for providing testing equipment, to Thom Porro from Sawbones and Jonathan Trottier from Synthes for sponsoring important materials.

## References

1. Davidian, K. Space Tourism Industry Emergence: Description and Data. *New Space* **8,** 87–102 (2022). https://doi.org/10.1089/space.2019.0040
2. Huh, J. & Kwon, S. A practical design approach for a single-stage sounding rocket to reach a target altitude. *Aeronaut. J.* **126,** 1084–1100 (2022). https://doi.org/10.1017/aer.2022.18
3. Nicholson, J., Makaram, N., Simpson, A. & Keating, J. Fracture nonunion in long bones: A literature review of risk factors and surgical management. *Injury* **52,** S3–S11 (2021). https://doi.org/10.1016/j.injury.2020.11.029
4. Genah, S., Monici, M. & Morbidelli, L. The Effect of Space Travel on Bone Metabolism: Considerations on Today's Major Challenges and Advances in Pharmacology. *J. Mol. Sci.* **22,** 4585 (2021). https://doi.org/10.3390/ijms22094585
5. Hadjkidakis, D. J. Bone Remodeling. *Ann. N. Y. Acad. Sci.* **96,** 385–396 (2006). https://doi.org/10.1196/annals.1365.035
6. Ott, S. M. Cortical or Trabecular Bone: What's the Difference? *Am. J. Nephrol.* **47,** 373–375 (2018). https://doi.org/10.1159/000489672
7. Madadi, F. Adult tibial shaft fractures – different patterns, various treatments and complications. *Med. Sci. Monit.* **17,** 640–645 (2011). https://doi.org/10.12659/msm.882049
8. The Royal Children's Hospital Melbourne. Clinical Practice Guidelines: Tibial shaft (diaphyseal) fracture — Emergency Department; https://www.rch.org.au/clinicalguide/guideline_index/fractures/tibial_shaft_emergency/
9. Isogai, K. et al. Young's moduli of subcutaneous tissues and muscles under different loads at the gluteal region calculated using ultrasonography. *J. Phys. Ther. Sci.* **34,** 777–783 (2022). https://doi.org/10.1589/jpts.34.777
10. Jovanovic, S. Applicability of bovine tibia as a model in research on various osteosynthesis techniques. *Period. Biol.* **112,** 59–62 (2010).
11. Li, Z., Wang, Q. & Liu, G. A Review of 3D Printed Bone Implants. *Micromachines* **13,** 528 (2022). https://doi.org/10.3390/mi13040528
12. Pacific Research Laboratory. Biomechanical Materials for Testing and Validation (2023); https://www.sawbones.com/biomechanical-product-info
13. Blue Origin. New Shepard (2023); https://www.blueorigin.com/new-shepard
14. Sarafin, T. *Vibration Testing of Small Satellites* tech. rep. (Instar Engineering and Consulting, Inc., 2017). https://s3vi.ndc.nasa.gov/ssri-kb/static/resources/Instar_Vibration_Testing.pdf.
15. Beer, F. P., Johnston Jr, E. R., DeWolf, J. T. & Mazurek, D. F. *Mechanics of Materials* (McGraw-Hill Education, 2020).
16. Maeda, K. Cortical thickness of the tibial diaphysisreveals age- and sex-related characteristicsbetween non-obese healthy young andelderly subjects depending on the tibialregions. *J. Exp. Orthop.* **7,** 1–11 (2020). https://doi.org/10.1159/000489672
17. International Organization for Standardization. Determination of Flexural Properties, Plastics (2019); https://www.iso.org/obp/ui/es/#iso:std:iso:178:ed-6:v1:en
18. Deckard, C. Using three-point bending to evaluate tibia bone strength in ovariectomized young mice. *J. Biol. Phys.* **43,** 139–148 (2017). https://doi.org/10.1007/s10867-016-9439-y
19. Norton, M. Bone glue – The final frontier for fracture repair and implantable device stabilization. *Int. J. Adhes. Adhes.* **102,** 102647 (2020). https://doi.org/10.1016/j.ijadhadh.2020.102647